Biosensors and Bioelectronics 131 (2019) 79–87

Contents lists available at ScienceDirect

Biosensors and Bioelectronics

journal homepage: www.elsevier.com/locate/bios

Cathodic "signal-on" photoelectrochemical aptasensor for chloramphenicol detection using hierarchical porous flower-like Bi-BiOI@C composite

Yuhan Zhu[a], Kai Yan[a], Zuwei Xu[b], Jinnan Wu[a], Jingdong Zhang[a,*]

[a] Key laboratory of Material Chemistry for Energy Conversion and Storage (Ministry of Education), School of Chemistry and Chemical Engineering, Huazhong University of Science and Technology, Luoyu Road 1037, Wuhan 430074, PR China

[b] State Key Laboratory of Coal Combustion, School of Energy and Power Engineering, Huazhong University of Science and Technology, Luoyu Road 1037, Wuhan 430074, PR China

ARTICLE INFO

Keywords:
Bi-BiOI@C
Surface plasmon resonance
Cathodic photocurrent
Aptasensor
Chloramphenicol

ABSTRACT

A novel p-type semiconductor-based cathodic "signal-on" photoelectrochemical (PEC) aptasensor was proposed for highly sensitive and selective detection of chloramphenicol (CAP). The photocathode was fabricated with hierarchical porous flower-like Bi-BiOI@C composite synthesized via a one-pot solvothermal method using glucose as both green reductant and carbon precursor. Due to the surface plasmon resonance (SPR) effect of Bi and high-conductivity of carbon, the composite exhibited an enhanced cathodic photocurrent as compared with pure BiOI or Bi-BiOI. When CAP-binding aptamer was immobilized as recognition element on Bi-BiOI@C modified electrode, a cathodic PEC aptasensor showing specific "signal-on" response to CAP was constructed. Some influencing factors such as coating amount of Bi-BiOI@C suspension, applied bias potential, and aptamer concentration were studied. Under the optimum conditions, the cathodic photocurrent of the constructed PEC aptasensor increased linearly with CAP concentration from 2 to 250 nM, with a detection limit (3S/N) of 0.79 nM. The proposed sensor was successfully applied to the determination of CAP in pharmaceutical tablet, eye drop and lake water samples.

1. Introduction

Photoelectrochemical (PEC) sensing has been a dynamically developing analytical method with attractive merits including fast response, high sensitivity, cost-effectiveness and permissible miniaturization (Zang et al., 2017; Zhang et al., 2017). Generally, the performance of photoresponsive materials plays a key role in PEC sensing. Although many n-type semiconductors such as TiO_2, ZnO and CdS quantum dots possessing high photoelectrocatalytic activity have been extensively employed to fabricate photoanodes for PEC sensing devices (Wang et al., 2009; Zhang et al., 2014a; Zhu et al., 2015), p-type semiconductors which are prone to interact with electron acceptors rather than electron donors have recently attracted much interest in developing cathodic PEC sensors (Fan et al., 2016; Teng et al., 2018; Wang et al., 2015a). In photocathodic sensing, a "signal-off" strategy based on electron blocking has usually been adopted for detection of non-electronic receptors, particularly in the aspect of bioassay, manifesting a photocurrent diminution by the analyte-induced steric hindrance or exciton trapping (Wang et al., 2012; Yan et al., 2015). Meanwhile, a "signal-on" architecture derived from direct photocatalytic reduction, enzyme or hemin-initiated signal amplification mechanism has also been established (Li et al., 2015; Wang et al., 2015b; Zhou et al., 2018). Actually, "signal-on" approach is preferable to "signal-off" way in terms of sensitivity and selectivity, owing to its lower background and reduction in the chance of appearing false positive response (Wang et al., 2015b; Zhang et al., 2012). However, cathodic "signal-on" PEC aptasensing has seldom been explored.

BiOI is a typical p-type semiconductor with a narrow band gap (~1.8 eV), which has high visible light activity (Gong et al., 2012; Hao et al., 2012). However, similar to other semiconductors, pure BiOI also suffers from the recombination of photogenerated electron-hole pairs which is unfavorable to the photocatalytic activity. It has been demonstrated that Au, Ag and Pt nanoparticles can improve the photocatalytic activity of BiOI through surface plasmon resonance (SPR) effect (Gan et al., 2016; Liu et al., 2012; Yu et al., 2010). Meanwhile, metallic Bi, which is cheaper and more readily available than noble metals, can also exhibit SPR effect similar to noble metals that can facilitate the generation, separation and transmission of photoinduced carriers in BiOI (Jiao et al., 2017; Ning et al., 2017). Actually, glucose can be employed as an excellent reducing agent for the synthesis of Bi

* Corresponding author.
E-mail address: zhangjd@mail.hust.edu.cn (J. Zhang).

https://doi.org/10.1016/j.bios.2019.02.008
Received 11 January 2019; Accepted 4 February 2019
Available online 18 February 2019
0956-5663/

nanoparticles modified BiOI via in situ reduction of partial Bi^{3+} into zero-valence bismuth during the synthetic process of BiOI (Yan et al., 2017). On the other hand, carbon nanomaterials including carbon nanotubes (Shu et al., 2014) and graphene (Wang et al., 2017a; Yan et al., 2015) have been cooperated with BiOI in fabricating photoelectrodes for PEC devices, due to their superior conductivity for efficient separation of photocarriers and improvement of PEC performance. Although satisfactory PEC performances are obtained, complex procedures with relatively long time for synthesis of carbon nanomaterials and additional mechanical mixing with photocatalysts are required in preparation of these composites. Actually, carbon incorporation can be easily implemented by adding carbon precursor (e.g. glucose) during the semiconductor manufacture process so as to improve electron transfer without time-consuming synthesis procedure (Guo et al., 2015; Ren et al., 2007).

Owing to its accessibility, low cost and high efficiency against infections, chloramphenicol (CAP) was commonly used in clinical medicine and animal husbandry as a broad-spectrum antibiotic (Gilmore, 1986; Pilehvar et al., 2012). However, CAP has mainly been limited for external use since its harmful side effects on human health and ecological risks were discovered (Lancaster et al., 1998; Wallace et al., 1975; Xu et al., 2013). The presence of CAP residues in animal-derived food products and wastewater samples has been frequently reported due to illegal use (Ferguson et al., 2005; Guo et al., 2017). It is still essential to develop rapid, sensitive and selective analytical methods to detect CAP. Recently, different photoanode-based PEC sensors have been developed for CAP determination (Liu et al., 2015; Sui et al., 2018; Wang et al., 2018). Our group has fabricated a label-free PEC aptasensor with nitrogen-doped graphene quantum dots which exhibited an increased photocurrent response with increasing the CAP concentration (Liu et al., 2015). Actually, CAP is a typical nitrobenzene derivative which can be reduced by electrochemical or PEC process. Although a number of cathodic electrochemical sensors for CAP detection have been demonstrated (Codognoto et al., 2010; Munawar et al., 2018; Pilehvar et al., 2012), cathodic PEC sensing of CAP has not been described so far.

In the present work, Bi-BiOI@C composite was successfully synthesized via a one-pot facile solvothermal process, in which glucose was added into the precursor solution of BiOI to serve as both green reductant and carbon precursor. The as-prepared Bi-BiOI@C displayed a hierarchical porous flower-like microstructure and an improved cathodic PEC performance due to SPR effect of Bi and carbon incorporation. We employed Bi-BiOI@C composite as photoactive material and CAP-binding aptamer as recognition element to explore a novel cathodic PEC aptasensing strategy to detect CAP. When CAP was present in analytical solution, it could be specifically captured by aptamer and then effectively accepted photogenerated electrons on Bi-BiOI@C to increase the cathodic photocurrent, as illustrated in Scheme 1. Thus, a cathodic "signal-on" PEC aptasensor for highly sensitive and selective detection of CAP was obtained.

2. Experimental section

2.1. Chemicals

CAP, doxycycline (DOX), chlortetracycline (CTC), neomycin (NEO), gentamicin (GEN), kanamycin (Kana), streptomycin (Strp), ofloxacin (OFL) and poly (diallyldimethylammonium chloride) (PDDA, MW 100000–200000, 20 wt% in H_2O) were obtained from Aladin Reagent Co., Ltd. (Shanghai, China). Bismuth nitrate pentahydrate (Bi $(NO_3)_3{\cdot}5H_2O$), potassium iodide (KI), polyvinylpyrrolidone (PVP, GR) and other reagents of analytical grade were acquired from Sinopharm Chemical Reagent Co., Ltd. (Shanghai, China). CAP-binding DNA aptamer used in this study with sequence of 5′-ACTTC AGTGA GTTGT CCCAC GGTCG GCGAG TCGGT GGTAG-3′ was synthesized by Shanghai Sangon Biotech Co., Ltd. (Shanghai, China). The aptamer stock solution was prepared with 0.01 M phosphate buffer solution (PBS, pH 8.0) and stored in refrigerator if not used. CAP eye drop was purchased from Handan Kangye Pharmaceutical Co., Ltd. (Handan, China), and CAP tablet was supplied by Anhui Golden Sun Biochemical Pharmaceutical Co., Ltd. (Fuyang, China). Doubly distilled water was used throughout the research work.

2.2. Synthesis of Bi-BiOI@C composite

The composite was prepared through a solvothermal method. Briefly, in a 100 mL Teflon-lined autoclave, 2 mmol Bi$(NO_3)_3{\cdot}5H_2O$ was rapidly added into 40 mL of ethylene glycol containing 2 mmol KI, 0.25 g PVP and 0.2 g glucose under vigorous stirring. After the obtained orange solution was stirred continuously for another 1 h at room temperature, the autoclave was sealed in a stainless steel tank and heated to 180 °C in an electric oven for 3 h under autogenous pressure. Then, the reactor was cooled to room temperature naturally. The product was collected by centrifugation, washed several times with deionized water and ethanol, and dried at 60 °C. The Bi-BiOI@C composite was dispersed in water to give a 2 mg mL^{-1} suspension under ultrasonic agitation. For comparison, pure BiOI was prepared by the same procedure except for the addition of glucose; and Bi-BiOI was synthesized by a long-time solvothermal reduction process which was carried out at 180 °C for 24 h in the absence of glucose as described previously (Chang et al., 2013).

2.3. Construction of PEC aptasensor

Before modification, the glass carbon electrode (GCE) surface was

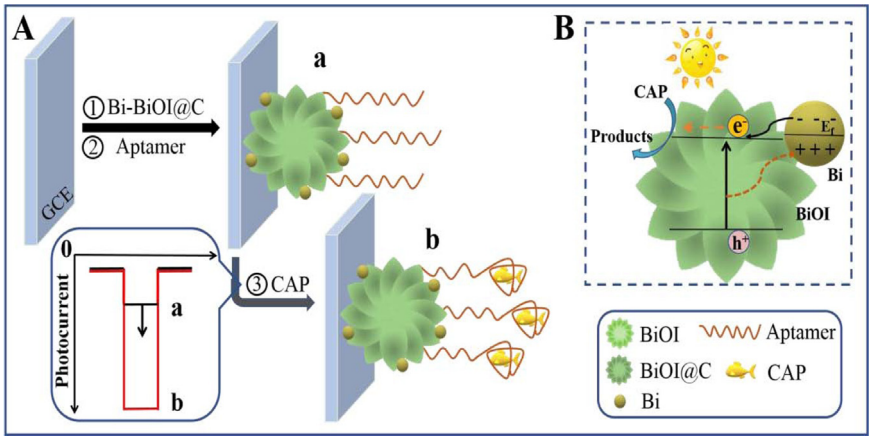

Scheme 1. Schematic illustration of fabricating cathodic "signal-on" PEC aptasensor on Bi-BiOI@C for CAP detection.

polished to a mirror-like smoothness with aqueous slurry of 0.05 μm alumina on a damp chamois, and then cleaned with ethanol and double distilled water successively. The GCE surface was sealed with Scotch tape with an exposed geometric area of 0.096 cm^2. Then, 10 μL of Bi-BiOI@C suspension was coated on exposed GCE surface and dried at 60 °C. The modified electrode was treated with 2% PDDA solution containing 0.5 mol L^{-1} NaCl to make the surface positively charged, followed by rinsing with distilled water to remove loosely adsorbed PDDA. After being dried with nitrogen gas, the electrode was incubated with 8 μL aptamer at a desired concentration at 40 °C for 2 h, ensuring the effective immobilization of negatively charged aptamer on hierarchical microsphere via electrostatic attraction. After carefully rinsing with 0.01 M PBS (pH 8.0) and drying naturally, the fabricated aptamer/Bi-BiOI@C/GCE was stored in refrigerator for further use.

2.4. Apparatus and procedure

The surface morphology and component analysis were evaluated by a Gemini 300 field emission scanning electron microscope (SEM) (Carl Zeiss, Germany) equipped with X-Max 50 energy dispersive spectroscopy (EDS) (Oxford, UK). The transmission electron microscopic (TEM) images were obtained on a Tecnai G2 20 TEM instrument (FEI, The Netherlands), and high-angle annular dark-field scanning transmission electron microscopic (HAADF-STEM) images as well as EDS spectra of selected regions were measured with a Talos F200X instrument (FEI, The Netherlands). The crystalline phases of the material compositions were analyzed by X-ray diffraction (XRD, Bruker Instruments, Germany) with Cu K_α radiation. The X-ray photoelectron spectra (XPS) were recorded on an AXIS ULTRA DLD-600W spectrometer (Kratos Company, England). The UV–visible absorption spectra were obtained with a TU-1900 spectrometer (Beijing Purkinje General Instrument Company, China).

The PEC measurements and electrochemical impedance spectra (EIS) were performed in a conventional three-electrode system using CHI830C and CHI660A electrochemical working stations (Shanghai Chenhua Instrument Co. Ltd., China), respectively. A CEL-S500/350 xenon lamp (CEAULIGHT Co., China) with an optical filter ($\lambda > 420$ nm) was employed as the irradiation source, and the distance between the light source and working electrode surface was 10 cm. EIS measurements were recorded in 0.5 M KCl solution containing 5.0 mM $K_3Fe(CN)_6/K_4Fe(CN)_6$ with the frequency range from 0.1 Hz to 100 kHz at a bias potential of 0.2 V (vs. SCE).

To study the PEC sensing performance, the aptasensor was incubated with 0.01 M PBS (pH 8.0) containing desired concentration of CAP at 40 °C for 2.0 h, followed by thoroughly rinsing with PBS. The electrode was then placed in a three-electrode cell containing 0.1 M Na_2SO_4 solution to serve as the working electrode. The photocurrent responses of the aptasensor before and after incubated with CAP were recorded via an on-off cycle of intermittent visible light irradiation.

The concentration of CAP samples determined by high-performance liquid chromatograph (HPLC) was carried out on an 1100 module system (Agilent, USA) with TC-C18 column (250 mm × 4.6 mm). The column temperature was 30 °C. The detection wavelength was set at 278 nm using a diode array detector (DAD). The mobile phase was a mixture of methanol and ultrapure water in the ratio of 55:45 (v/v). The flow rate of mobile phase was 1 mL min^{-1}.

3. Results and discussion

3.1. Characterization of Bi-BiOI@C composite

The morphology of as-prepared Bi-BiOI@C composite was observed by SEM. As shown in Fig. 1A, abundant microspheres in the size range of 0.9–1.3 μm form a porous film on the modified electrode surface. Further observation indicates that the microspheres display hierarchical flower-like architecture and some small balls are decorated on microspheres (inset of Fig. 1A). In contrast, pure BiOI and Bi-BiOI exhibit uneven microspheres with relatively larger size (Fig. S1). In addition, EDS analysis of the composite on a silicon wafer was carried out to verify the elemental distribution of Bi, I, O and C for Bi-BiOI@C. As shown in Fig. 1B, the content of Bi element is relatively superior to I and O, due to the partial presence of nulvalent Bi. Such morphology of Bi-BiOI@C should be favorable to construction of PEC sensor. (1) Three-dimensional porous structure can provide better PEC performance than its bulk counterpart, owing to the anti-aggregation ability, large surface area and abundant transmission channels to the active sites of photogenerated carriers (Fei et al., 2011; Xiao et al., 2010; Zhong et al., 2006). (2) Hierarchical frame is an ideal support for the immobilization of microparticles and recognition element (Gong et al., 2015; Peng et al., 2014).

Meanwhile, the flower-like microspheres decorated with small balls can also be seen in the TEM image (Fig. 1C). The high-resolution transmission electron microscopic (HRTEM) image clearly reveals the lattice spacing of 0.301 nm and 0.328 nm, corresponding to the (012) planes of BiOI and Bi, respectively (Fig. 1D). Besides, a lattice spacing of 0.337 nm belonging to the (002) planes of graphite phase is observed, suggesting the presence of carbon in the composite. On the other hand, HAADF-STEM observation provides further insight into the morphology and structure of the composite (Fig. 1E). The EDS analysis combined with HAADF-STEM in selected regions confirms that the flower-like microsphere corresponds to BiOI while the attached small ball is assigned to Bi, and carbon is only distributed on BiOI microsphere. Additionally, the Bi ball attached to BiOI surface and C element distributed throughout the petals of BiOI microsphere can be directly observed by the corresponding EDS elemental mapping of HAADF-STEM image (Fig. 1F).

The crystalline nature and composition of the as-synthesized materials were analyzed by XRD. As shown in curve a in Fig. 2A, the diffraction peaks marked with a rhombus symbol match well with the tetragonal phase of BiOI (JCPDS card no. 73-2062). In Bi-BiOI sample, the corresponding peaks of BiOI in the product are weakened, accompanied by the emergence of new diffraction peaks (curve b in Fig. 2A). The peaks marked with a dot-form symbol can be assigned to the rhombohedral phase of Bi (JCPDS card no. 44-1246), indicating that some amount of Bi^{3+} is converted to Bi by long-time solvothermal reduction (Chang et al., 2013). With the addition of glucose in the reactive solution, the diffraction peaks for both BiOI and Bi are observed since some amount of Bi^{3+} is reduced by glucose (curve c in Fig. 2A). Besides, three peaks at 26.8°, 44.5°, and 54.5° are assigned to the (002), (101) and (004) crystal planes of graphite carbon, respectively (JCPDS card No. 08-0415), which is supplied by the carbonization of glucose. Accordingly, the XRD results also indicate that the composite of Bi-BiOI@C is successfully formed by the solvothermal method.

To further ascertain the surface chemical compositions and valence states of the as-prepared composite, XPS analysis was carried out. In Fig. 2B, the XPS survey spectrum of Bi-BiOI@C clearly indicates that only Bi, O, and I and C elements are detected in the sample. Fig. 2C shows the typical high-resolution XPS spectrum of Bi 4f. As can be seen, two peaks with binding energies of 163.8 and 158.5 eV are assigned to Bi $4f_{5/2}$ and Bi $4f_{7/2}$ of trivalent bismuth element, respectively. Besides, two smaller fitting peaks centered at 162.2 and 155.8 eV corresponding to metallic Bi at zero valence state are observed (Bhachu et al., 2016; Jing et al., 2018), which can be ascribed to the mild reduction of partial bismuth ions by glucose. After deconvolution, the O 1s spectrum can be fitted with three peaks (Fig. 2D). The dominant peak at 530.4 eV belongs to the Bi–O bond of BiOI, and the other two peaks at 529.3 and 532.1 eV suggest the presence of surface hydroxyl groups and adsorbed H_2O (Brook et al., 2007; Liu et al., 2012). The XPS spectrum of I 3d exhibits two peaks at 629.6 and 618.1 eV (Fig. 2E), which are assigned to I $3d_{3/2}$ and I $3d_{5/2}$, respectively. As for C1s spectrum (Fig. 2F), the peak around 284.9 eV possibly states the existence of the characteristic sp^2 carbon (C–C) in graphite (Dong et al., 2012; Titirici et al., 2007),

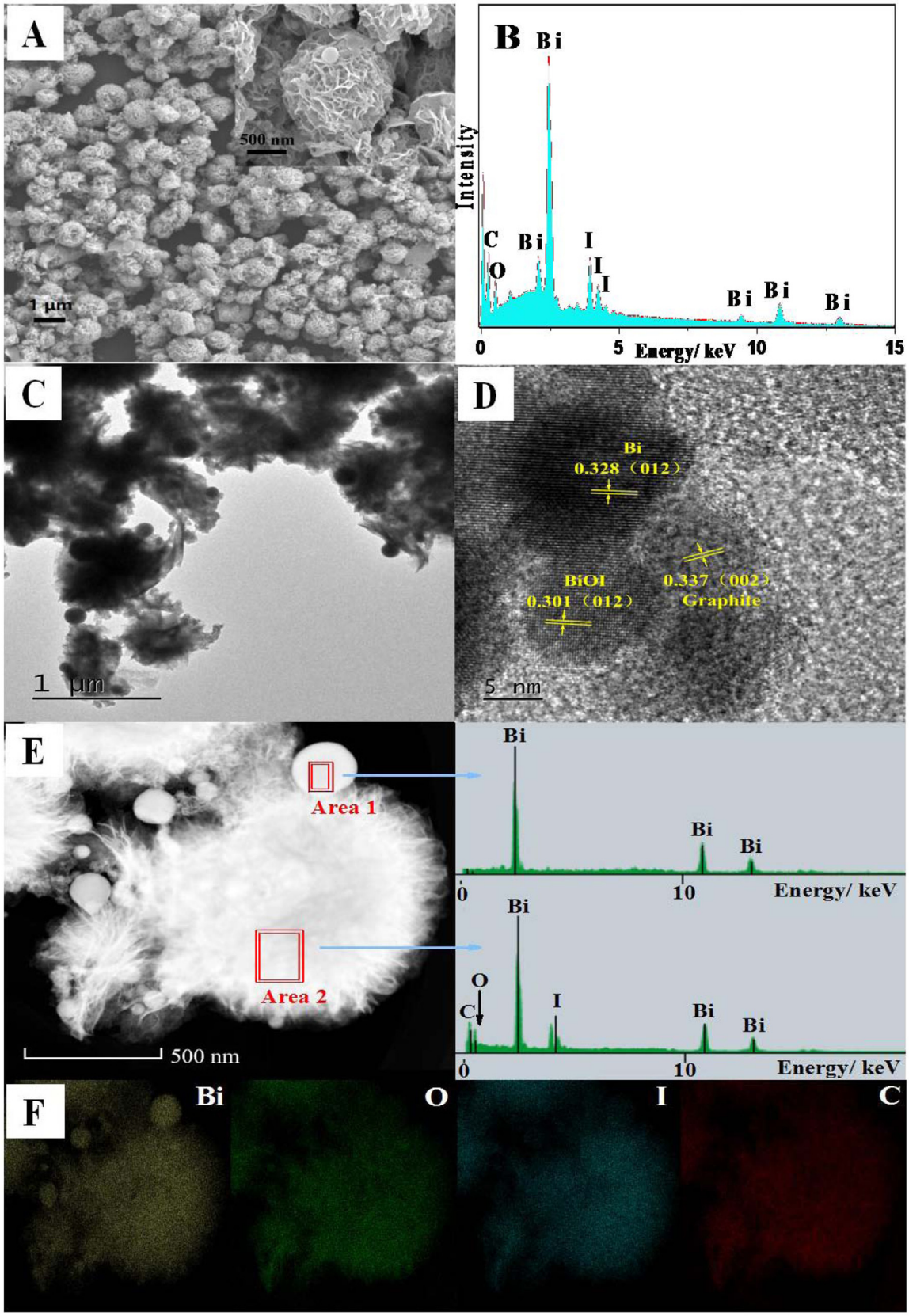

Fig. 1. (A) SEM images and (B) EDS analysis of Bi-BiOI@C. (C) TEM and (D) HRTEM images of Bi-BiOI@C. (E) HAADF-STEM image of Bi-BiOI@C and EDS spectra of selected regions. (F) Corresponding EDS elemental mapping of HAADF-STEM image.

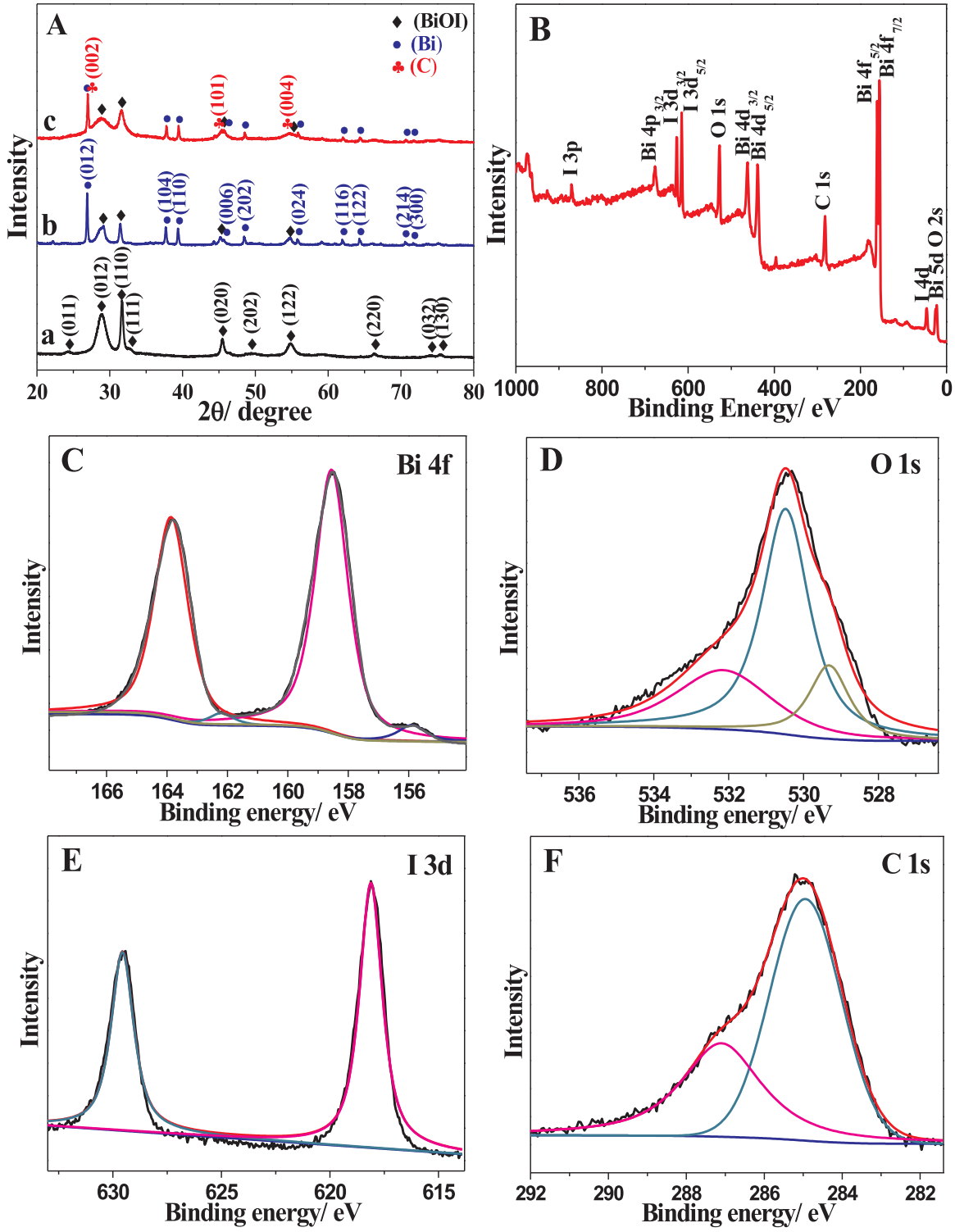

Fig. 2. (A) XRD patterns of (a) BiOI, (b) Bi-BiOI and (c) Bi-BiOI@C composite. (B) XPS survey spectrum of Bi-BiOI@C and high-resolution XPS spectra for (C) Bi 4f, (D) O 1s, (E) I 3d and (F) C 1s.

but it could also be attributed to the adventitious carbon used for calibration from the XPS instrument. In addition, the peak centered at 287.1 eV indicates the presence of C–O bond with a slight shift to standard reference value (286 eV), which may be caused by the particular chemical environment. These results are in agreement with those of HRTEM and XRD, further confirming the successful preparation of designed materials with the coexistence of BiOI, Bi and carbon.

3.2. Optical, photocurrent and impedance analysis

The optical absorption characteristics of the as-synthesized samples are shown in Fig. 3A. In comparison with orange BiOI (curve a in Fig. 3A), yellow-green colored Bi-BiOI (curve b in Fig. 3A) has much stronger UV–visible absorption because of the SPR effect between BiOI and plasmonic Bi. For dark-green Bi-BiOI@C composite, the absorption shows further promotion in the visible light region (curve c in Fig. 3A).

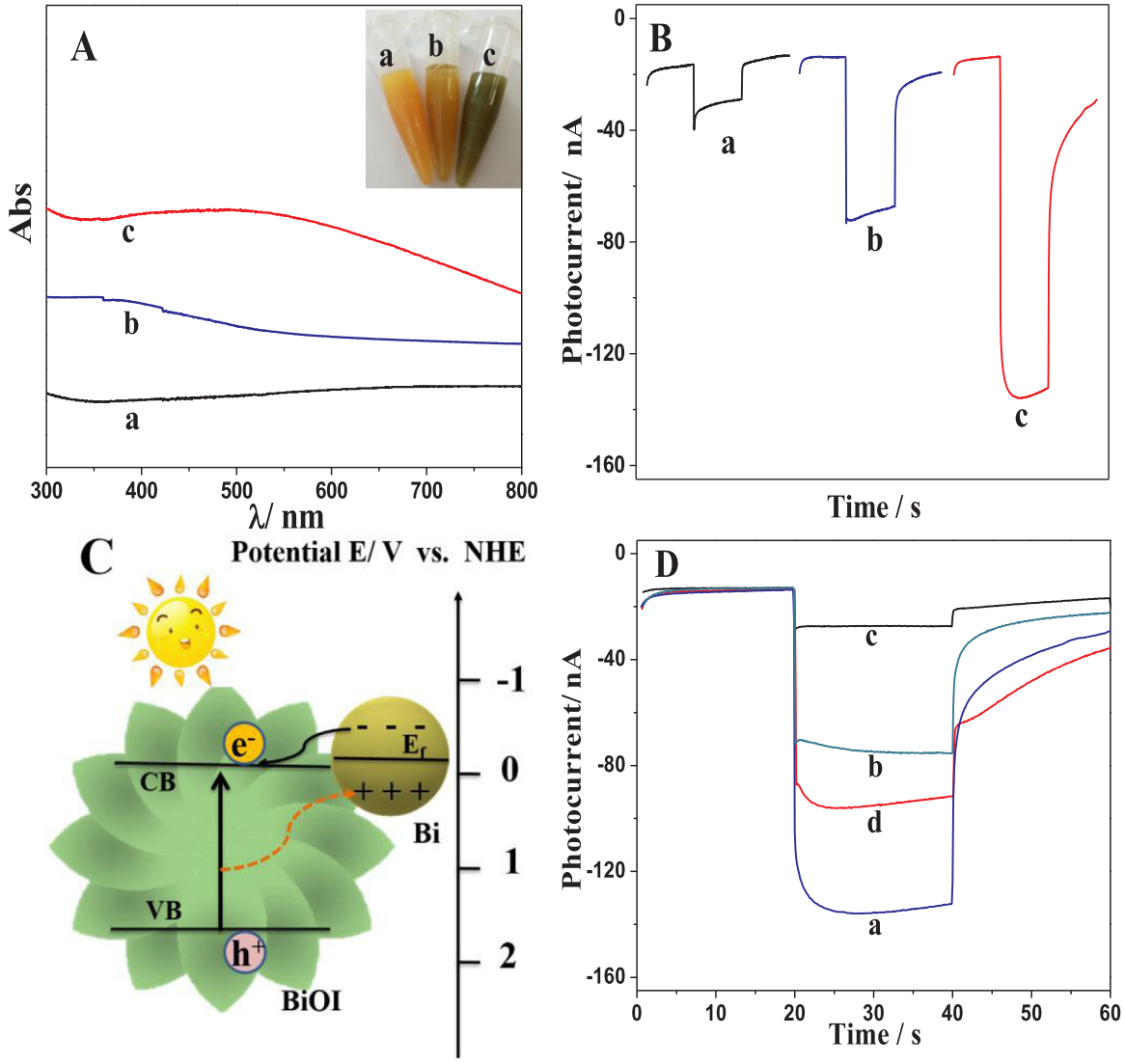

Fig. 3. (A) UV–visible absorption spectra of (a) BiOI, (b) Bi-BiOI and (c) Bi-BiOI@C composite. (B) Photocurrent responses of (a) BiOI/GCE, (b) Bi-BiOI/GCE and (c) Bi-BiOI@C/GCE recorded in 0.1 M Na_2SO_4 at a bias potential of −0.15 V. (C) Energy band diagram for the separation mechanism of photogenerated carriers caused by SPR effect between Bi and BiOI under visible-light irradiation. CB, conduction band; VB, valence band. (D) Photocurrent responses of different modified electrodes recorded in 0.1 M Na_2SO_4 at −0.15 V: (a) Bi-BiOI@C/GCE, (b) aptamer/Bi-BiOI@C/GCE, (c) aptamer/Bi-BiOI@C/GCE in 0.1 M Na_2SO_4 solution (deaerated), (d) aptamer/Bi-BiOI@C/GCE incubated with 200 nM CAP in 0.1 M Na_2SO_4 solution (deaerated).

On the other hand, the photocurrents of various modified electrodes were measured under visible light irradiation. As can be seen in Fig. 3B, the Bi-BiOI@C modified electrode exhibits higher cathodic photocurrent than BiOI/GCE and Bi-BiOI/GCE, consistent with its effective optical absorption. Fig. 3C illustrates the transfer mechanism of photogenerated carriers on the composite. From the energy band diagram, the conduction band (CB) of BiOI is more positive than the Fermi level of metallic Bi (-0.17 eV, vs. NHE) (Huang et al., 2016). Because of the SPR effect, under illumination of visible light, the excited 6sp electrons of Bi would migrate to the CB of BiOI thermodynamically. That is, the SPR effect of Bi could reduce the recombination of the photogenerated electron-hole pairs and increase the lifetime of the carriers in BiOI semiconductor. Moreover, the local electromagnetic field caused by SPR effect (Wang et al., 2017b) and the favorable conductivity of the supporting carbon (Zhang et al., 2014b; Zhu et al., 2017) could facilitate the interfacial electron transfer process, resulting in promotion of the visible-light photocatalyst performance.

Further, the PEC responses of the as-fabricated photocathode before (curve a in Fig. 3D) and after (curve b in Fig. 3D) immobilization of CAP-binding aptamer were compared. As can be seen, the photocurrent of Bi-BiOI@C/GCE declines obviously after aptamer is immobilized. This can be ascribed to enhanced steric hindrance of aptamer for electron transfer between the photoelectric material and electron acceptor. Moreover, the photocurrent of aptamer/Bi-BiOI@C/GCE further decreases when the electrolyte is deaerated with nitrogen (curve c in Fig. 3D), declaring that dissolved oxygen can act as electron acceptor in the photocathodic process. After the aptamer/Bi-BiOI@C/GCE is incubated with CAP, the photocurrent in deaerated electrolyte significantly enhances (curve d in Fig. 3D), meaning that captured CAP molecules act as electron acceptor participating in the cathodic process. That is, the *p*-nitrophenyl group in CAP molecule can feasibly consume photogenerated electrons for the generation of cathodic photocurrent. Therefore, it is necessary to exclude the dissolved oxygen in the electrolyte during the CAP sensing.

On the other hand, EIS analysis using $[Fe(CN)_6]^{3-/4-}$ as redox probe was carried out to study the interfacial electrochemical properties of modified electrodes. According to the semicircle diameter of Nyquist plots at high frequency region, the electron-transfer resistance (R_{et}) of modified electrode was evaluated. As illustrated in Fig. S2, the R_{et} value of bare GCE increases after coating with BiOI, owing to the low

conductivity of semiconductor. By contrast, the Bi-BiOI modified electrode exhibits smaller R_{et} value than BiOI/GCE, meaning that the electron transfer ability of the modified electrode is improved after some amount of BiOI is converted to metallic Bi. When carbon is incorporated with Bi-BiOI, the R_{et} value is further decreased, which is found to be even lower than that of GCE, demonstrating the role of carbon with high electronic conductivity in facilitating the electron transfer rate between electrode and redox species. Nevertheless, after aptamer is immobilized on Bi-BiOI@C/GCE, the R_{et} value dramatically increases, attributed to the electrostatic repulsion between negatively charged phosphate backbone of aptamer molecules and redox species. This result confirms the effective assembly of aptamer on Bi-BiOI@C electrode surface.

3.3. Optimization of amount of Bi-BiOI@C, bias potential, and aptamer concentration

The influences of the coating amount of Bi-BiOI@C suspension and applied bias potential on the PEC response of Bi-BiOI@C/GCE were studied. As can be seen in Fig. S3, the photocurrent increases with increasing the amount of composite from 4 to 10 μL and then becomes saturation with further increased amount. Thus, 10 μL of suspension solution was chosen as the optimized amount for fabricating the modified electrode. On the other hand, Fig. S4 shows that the photocurrent response increases with changing the bias potential from 0 to −0.15 V, indicating that the electron acceptor molecules are efficiently reduced under negative potential and the recombination probability of the photogenerated electron-hole pairs are considerably suppressed (Zhu et al., 2017). However, the photocurrent response of Bi-BiOI@C/GCE obviously declines when the applied potential is more negative than −0.15 V. This can be ascribed to the increase of dark current with increasing the negative potential. It is believed that dark current should be minimized so as to ensure higher signal-background ratio of photodetector (Teng et al., 2018). Therefore, −0.15 V was applied during the photocurrent measurement.

For aptasensor, it is widely accepted that the aptamer concentration has an obvious impact on the response. Herein, we investigated the optimum concentration of CAP-binding aptamer immobilized on the electrode surface by the photocurrent difference (ΔPI) before and after incubation with 200 nM CAP. The PEC responses of several aptasensors fabricated with different aptamer concentrations from 0.5 to 3 μM are compared. As shown in Fig. S5, the maximal ΔPI value is obtained with increasing the aptamer concentration up to 1.5 μM. When the aptamer concentration is higher than 1.5 μM, the PEC response of the aptasensor toward CAP declines. This can be ascribed to the fact that excessive amount of aptamer molecules on the electrode surface provides not only saturated active sites but also additional steric hindrance. Accordingly, 1.5 μM aptamer was employed as the optimum concentration to construct the sensor.

3.4. PEC aptasensing of CAP

The aptamer/Bi-BiOI@C/GCE was employed as PEC aptasensor for the determination of CAP. The PEC measurements were carried out in deaerated electrolyte under optimized experimental conditions. Fig. 4A demonstrates the photocurrent responses of aptamer/Bi-BiOI@C/GCE toward CAP at different concentrations. The cathodic photocurrent increases with the increase of CAP concentration, manifesting more captured CAP molecules are devoted to the PEC process. The PEC response of the sensor is found to be linearly proportional to the CAP concentration in the range of 2–250 nM (inset of Fig. 4A). The linear regression equation can be expressed as $\Delta PI/\mathrm{nA} = 0.234C/\mathrm{nM} + 14.42$ (correlation coefficient $R^2 = 0.998$). In addition, a low detection limit (3S/N) of 0.79 nM is estimated, which is superior to many previously reported CAP sensors (Table S1). Moreover, the calibration sensitivity of the proposed sensor is 0.234 A M^{-1}, comparable to most of these

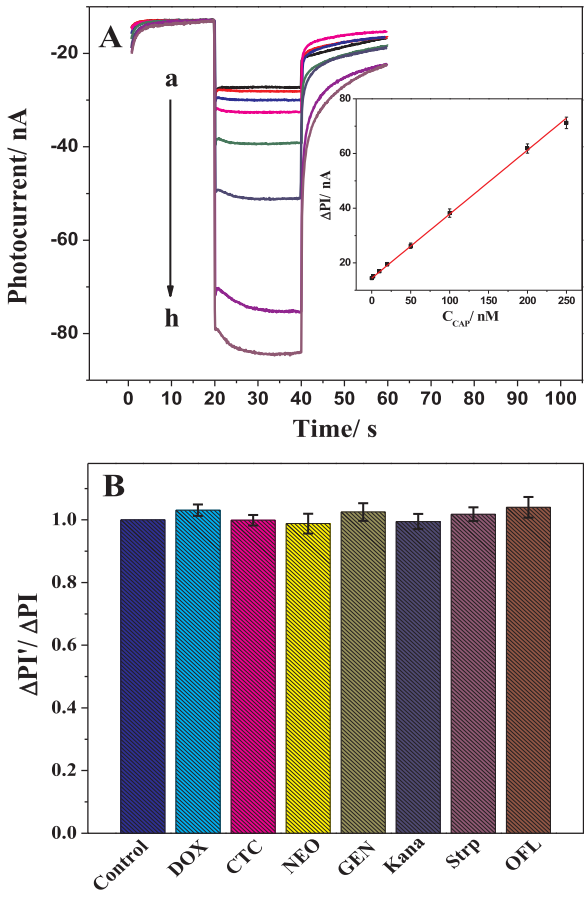

Fig. 4. (A) Photocurrent responses of the fabricated aptasensor in 0.1 M Na_2SO_4 solution (deaerated) after incubation with different concentrations of CAP: (a) 0, (b) 2, (c) 10, (d) 20, (e) 50, (f) 100, (g) 200, (h) 250 nM. Inset: calibration curve for CAP on the PEC sensor. Error bars are derived from the standard deviation of three measurements. (B) Histogram for ΔPI obtained on PEC sensor incubation with 200 nM CAP solution containing equal amount of other antibiotics, respectively. Error bars are derived from the standard deviation of three measurements.

reported CAP sensors.

The selectivity of the proposed PEC sensor was then evaluated, and the interference studies were carried out by analyzing the photocurrent response towards 200 nM CAP under optimum conditions with the addition of same concentration of some other antibiotics (such as DOX, CTC, NEO, GEN, Kana, Strp, OFL). As can be seen in Fig. 4B, all these species have no obvious interference in the determination of CAP. The result demonstrates the excellent selectivity of the aptasensor, owing to the specific interaction of aptamer with target CAP molecules. Additionally, as aforementioned, the photocathode prefers to interact with electron acceptor and possesses anti-interference ability against oxidation reactions of reductive substances occurring at the photoanode interface, which is favorable to improve the selectivity.

The reproducibility of the PEC aptasensor toward CAP was investigated by assessing the responses of five independently prepared electrodes. A relative standard deviation (RSD) of 2.28% is obtained for the detection, implying a good reproducibility of the proposed sensor. Moreover, after a storage time of twenty days in a refrigerator at 4 °C, no obvious change in the photocurrent response of the aptamer/Bi-BiOI@C/GCE is observed, thereby revealing high stability of the sensor.

3.5. Applications of aptasensor

To confirm the feasibility in real samples, the proposed PEC aptasensor was applied to CAP determination in pharmaceutical tablet, eye

Table 1
Assay of CAP in real samples by the proposed method compared with HPLC analysis (n = 3).

Sample	Claimed value (mg)	Found by proposed sensor (mg ± SD)	Found by HPLC (mg ± SD)	Relative difference (%)
Tablet	250	253.72 ± 3.70	256.75 ± 2.52	1.18
Eye drop	20	18.77 ± 0.42	19.03 ± 0.29	1.34

drop and lake water samples.

Prior to analysis, the commercial tablet was removed the layer of sugar coat and ground to fine powder. Then, the powder was accurately weighed and dissolved in 0.01 M hydrochloric acid, followed by filtering out the precipitate. The filtrate and eye drop were appropriately diluted with a mixture of methanol and water (55:45, v/v), respectively. After homogenizing, the samples were filtered by 0.22-μm nylon membrane filters. The results of the proposed PEC aptasensor and HPLC contrastive analysis are listed in Table 1. The result of PEC sensor shows that the CAP content in each tablet is 253.72 ± 3.70 mg, consistent with 256.75 ± 2.52 mg obtained by HPLC. Meanwhile, the PEC result gives that CAP content in each bottle (8 mL) of eye drop is 18.77 ± 0.42 mg, showing a good agreement with the result (19.03 ± 0.29 mg) analyzed by HPLC. The relative difference percentages of two methods for the CAP detection in both of tablet and eye drop are less than 1.4%, meaning that the proposed aptasensor can realize the rapid and sensitive detection of CAP in real samples with an acceptable accuracy.

On the other hand, the PEC aptasensor was employed to analyze CAP in environmental water samples collected from two lakes in Wuhan City using the standard addition method. Table S2 shows the recoveries of the proposed method are between 98.98% and 101.35%, indicating the reliability of the proposed method for CAP determination in environmental samples.

4. Conclusions

In this work, Bi-BiOI@C composite with hierarchical porous flower-like morphology was prepared via a facile solvothermal process and employed as photoactive material for fabricating a PEC sensing platform. The in situ introduction of Bi metal with SPR effect and carbon with high conductivity in BiOI was realized simultaneously by adding suitable glucose, leading to preferable cathodic photocurrent response. Meanwhile, the Bi-BiOI@C was coupled with aptamer which could provide specific recognition ability for CAP. On the basis of cathodic "signal-on" strategy, a novel PEC aptasensor for highly sensitive and selective detection of CAP with desirable reproducibility and stability was successfully developed. It is believed that exploring p-type semiconductor-based cathodic PEC sensors can not only exert the anti-interference capability to reductive substances, but also provide a comprehensive scope for sensing development. Moreover, this work demonstrates the perspective of glucose as mild reducing agent and carbon source for preparing high-performance PEC materials.

Acknowledgements

This work was supported by the National Natural Science Foundation of China (Grant No. 61571198) and the opening fund of Hubei Key Laboratory of Bioinorganic Chemistry & Materia Medica (Grant No. BCMM201704). We also thank the Analytical and Testing Center of Huazhong University of Science and Technology for help in materials characterization.

Declaration of interest statement

We declare that we do not have any commercial or associative interest in connection with this work.

Appendix A. Supporting information

Supplementary data associated with this article can be found in the online version at doi.org/10.1016/j.bios.2019.02.008.

References

Bhachu, D.S., Moniz, S.J., Sathasivam, S., Scanlon, D.O., Walsh, A., Bawaked, S.M., Mokhtar, M., Obaid, A.Y., Parkin, I.P., Tang, J., Carmalt, C.J., 2016. Chem. Sci. 7, 4832–4841.
Brook, L.A., Evans, P., Foster, H.A., Pemble, M.E., Steele, A., Sheel, D.W., Yates, H.M., 2007. J. Photochem. Photobiol. A 187, 53–63.
Chang, C., Zhu, L., Fu, Y., Chu, X., 2013. Chem. Eng. J. 233, 305–314.
Codognoto, L., Winter, E., Doretto, K.M., Monteiro, G.B., Rath, S., 2010. Microchim. Acta 169, 345–351.
Dong, Y., Wang, R., Li, H., Shao, J., Chi, Y., Lin, X., Chen, G., 2012. Carbon 50, 2810–2815.
Fan, G.C., Shi, X.M., Zhang, J.R., Zhu, J.J., 2016. Anal. Chem. 88, 10352–10356.
Fei, J., Cui, Y., Zhao, J., Gao, L., Yang, Y., Li, J., 2011. J. Mater. Chem. 21, 11742–11746.
Ferguson, J., Baxter, A., Young, P., Kennedy, G., Elliott, C., Weigel, S., Gatermann, R., Ashwin, H., Stead, S., Sharman, M., 2005. Anal. Chim. Acta 529, 109–113.
Gan, J., Rajeeva, B.B., Wu, Z., Penley, D., Zheng, Y., 2016. Electrochim. Acta 219, 20–27.
Gilmore, A., 1986. CMAJ: Can. Med. Assoc. J. 134, 423.
Gong, J., Fang, T., Peng, D., Li, A., Zhang, L., 2015. Biosens. Bioelectron. 73, 256–263.
Gong, J., Wang, X., Li, X., Wang, K., 2012. Biosens. Bioelectron. 38, 43–49.
Guo, N., Wang, Y., Yan, L., Wang, X., Wang, M., Xu, H., Wang, S., 2017. Water Res. 117, 95–101.
Guo, Y., Li, J., Chen, M., Gao, G., 2015. J. Power Sources 273, 804–809.
Hao, R., Xiao, X., Zuo, X., Nan, J., Zhang, W., 2012. J. Hazard. Mater. 209, 137–145.
Huang, Y., Kang, S., Yang, Y., Qin, H., Ni, Z., Yang, S., Li, X., 2016. Appl. Catal. B 196, 89–99.
Jiao, Z., Shang, M., Liu, J., Lu, G., Wang, X., Bi, Y., 2017. Nano Energy 31, 96–104.
Jing, Q., Feng, X., Pan, J., Chen, L., Liu, Y., 2018. Dalton Trans. 47, 2602–2609.
Lancaster, T., Swart, A.M., Jick, H., 1998. BMJ 316, 667.
Li, Z., Xin, Y., Zhang, Z., 2015. Anal. Chem. 87, 10491–10497.
Liu, H., Cao, W., Su, Y., Wang, Y., Wang, X., 2012. Appl. Catal. B 111, 271–279.
Liu, Y., Yan, K., Okoth, O.K., Zhang, J., 2015. Biosens. Bioelectron. 74, 1016–1021.
Munawar, A., Tahir, M.A., Shaheen, A., Lieberzeit, P.A., Khan, W.S., Bajwa, S.Z., 2018. J. Hazard. Mater. 342, 96–106.
Ning, S., Lin, H., Tong, Y., Zhang, X., Lin, Q., Zhang, Y., Long, J., Wang, X., 2017. Appl. Catal. B 204, 1–10.
Peng, D., Li, X., Zhang, L., Gong, J., 2014. Electrochem. Commun. 47, 9–12.
Pilehvar, S., Mehta, J., Dardenne, F., Robbens, J., Blust, R., Wael, K.D., 2012. Anal. Chem. 84, 6753–6758.
Ren, W., Ai, Z., Jia, F., Zhang, L., Fan, X., Zou, Z., 2007. Appl. Catal. B 69, 138–144.
Shu, D., Wu, J., Gong, Y., Li, S., Hu, L., Yang, Y., He, C., 2014. Catal. Today 224, 13–20.
Sui, C., Zhou, Y., Wang, M., Yin, H., Wang, P., Ai, S., 2018. Sens. Actuators B 266, 514–521.
Teng, F., Hu, K., Ouyang, W., Fang, X., 2018. Adv. Mater. 1706262.
Titirici, M.M., Thomas, A., Yu, S.H., Müller, J.O., Antonietti, M., 2007. Chem. Mater. 19, 4205–4212.
Wallace, D.C., Bunn, C.L., Eisenstadt, J.M., 1975. J. Cell Biol. 67, 174–188.
Wang, G.L., Gu, T.T., Dong, Y.M., Wu, X.M., Li, Z.J., 2015a. Electrochem. Commun. 61, 117–120.
Wang, G.L., Shu, J.X., Dong, Y.M., Wu, X.M., Zhao, W.W., Xu, J.J., Chen, H.Y., 2015b. Anal. Chem. 87, 2892–2900.
Wang, G.L., Xu, J.J., Chen, H.Y., 2009. Biosens. Bioelectron. 24, 2494–2498.
Wang, H., Liang, Y., Liu, L., Hu, J., Wu, P., Cui, W., 2017a. Appl. Catal. B 208, 22–34. https://www.sciencedirect.com/science/article/pii/S0926337317301662.
Wang, P., Ma, X., Su, M., Hao, Q., Lei, J., Ju, H., 2012. Chem. Commun. 48, 10216–10218. https://pubs.rsc.org/en/Content/ArticleLanding/2012/CC/c2cc35643k#!divAbstract.
Wang, Q., He, J., Shi, Y., Zhang, S., Niu, T., She, H., Bi, Y., 2017b. Chem. Eng. J. 326, 411–418.
Wang, Y., Bian, F., Qin, X., Wang, Q., 2018. Microchim. Acta 185, 161. https://link.springer.com/article/10.1007/s00604-018-2711-z.
Xiao, X., Zhang, W.D., 2010. J. Mater. Chem. 20, 5866–5870.
Xu, W., Yan, W., Li, X., Zou, Y., Chen, X., Huang, W., Miao, L., Zhang, R., Zhang, G., Zou, S., 2013. Environ. Pollut. 182, 402–407.
Yan, K., Liu, Y., Yang, Y., Zhang, J., 2015. Anal. Chem. 87, 12215–12220.
Yan, P., Xu, L., Cheng, X., Qian, J., Li, H., Xia, J., Zhang, Q., Hua, M., Li, H., 2017. J. Electroanal. Chem. 804, 64–71.
Yu, C., Jimmy, C.Y., Fan, C., Wen, H., Hu, S., 2010. Mater. Sci. Eng. B 166, 213–219.
Zang, Y., Lei, J., Ju, H., 2017. Biosens. Bioelectron. 96, 8–16.

Zhang, B., Lu, L., Hu, Q., Huang, F., Lin, Z., 2014a. Biosens. Bioelectron. 56, 243–249.
Zhang, N., Zhang, L., Ruan, Y.F., Zhao, W.W., Xu, J.J., Chen, H.Y., 2017. Biosens. Bioelectron. 94, 207–218. http://refhub.elsevier.com/S0956-5663(19)30108-3/sbref47.
Zhang, P., Sun, F., Xiang, Z., Shen, Z., Yun, J., Cao, D., 2014b. Energy Environ. Sci. 7, 442–450. http://refhub.elsevier.com/S0956-5663(19)30108-3/sbref48.
Zhang, X., Xu, Y., Yang, Y., Jin, X., Ye, S., Zhang, S., Jiang, L., 2012. Chem. Eur. J. 18, 16411–16418.
Zhong, L.S., Hu, J.S., Liang, H.P., Cao, A.M., Song, W.G., Wan, L.J., 2006. Adv. Mater. 18, 2426–2431.
Zhou, Q., Lin, Y., Zhang, K., Li, M., Tang, D., 2018. Biosens. Bioelectron. 101, 146–152.
Zhu, Y., Xu, Z., Yan, K., Zhao, H., Zhang, J., 2017. ACS Appl. Mater. Interfaces 9, 40452–40460.
Zhu, Y., Yan, K., Liu, Y., Zhang, J., 2015. Anal. Chim. Acta 884, 29–36.